ACS APPLIED MATERIALS & INTERFACES

RESEARCH ARTICLE

www.acsami.org

Facile Construction of High-Electrocatalytic Bilayer Counter Electrode for Efficient Dye-Sensitized Solar Cells

Feng Hao,[†] Hong Lin,[*,†] Yizhu Liu,[†] Ning Wang,[‡] Wendi Li,[§] and Jianbao Li[†,⊥]

[†]State Key Laboratory of New Ceramics & Fine Processing, Department of Material Science and Engineering, Tsinghua University, Beijing 100084, PR China

[‡]State Key Laboratory of Electronic Thin Films and Integrated Devices, University of Electronic Science and Technology of China, Chengdu 610054, PR China

[§]Department of Material Physics and Chemistry, University of Science & Technology Beijing, Beijing 100083, PR China

[⊥]Key Laboratory of Ministry of Education for Application Technology of Chemical Materials in Hainan Superior Resources, College of Materials Science and Chemical Engineering, Hainan University, Haikou 570228, PR China

ABSTRACT: To improve the mechanical rigidity of the electrocatalyst and assure a higher number density of catalytic sites of the counter electrode in dye-sensitized solar cells (DSCs), we have extended widely applied titanium tetrachloride treatment to construct a rough scaffolding underlayer for the platinized counter electrode. Field-emission scanning electron microscopy and atomic force microscopy images clearly depicted the platinum nanoparticles with a diameter of ca. 10 nm homogeneously distributed on the scaffolding underlayer of the bilayer counter electrode and thus led to a characteristically high surface roughness. The electocatalytic activity of this novel bilayer counter electrode was measured and compared with the corresponding properties of conventional sputtered Pt electrode. Interestingly, electrochemical impedance spectroscopy and cyclic voltammetry measurements further demonstrated the notably larger electrochemical active surface area and thereby higher electrocatalytic activity of the bilayer counter electrode. Consequently, under standard 1 sun illumination (100 mW cm^{-2}, AM 1.5), device with this bilayer counter electrode achieved a considerably improved fill factor of 0.67 and overall energy conversion efficiency of 7.09%, which was apparently higher than that of 0.60 and 6.37% for sputterd Pt electrode. Therefore, this present method paves a facile and inexpensive way to prepare high-electrocatalytic bilayer counter electrode in DSCs.

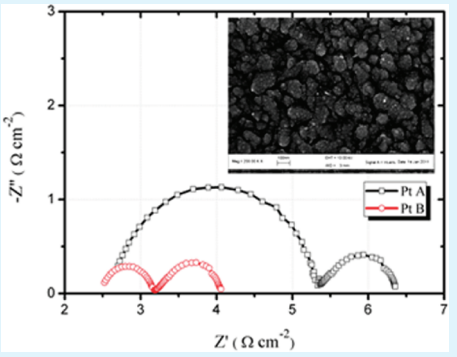

KEYWORDS: titanium tetrachloride treatment, electrocatalytic activity, counter electrode, electrochemical active surface area, charge transfer resistance, dye-sensitized solar cells

1. INTRODUCTION

Worldwide interest towards dye-sensitized solar cell (DSC) as a credible alternative to conventional silicon-based solar cell has been consistently motivated because of its practical merits such as inexpensive raw materials and fabrication costs, eco-friendly characteristics, and high power conversion efficiencies.[1−4] These cells normally consist of transparent conducting oxide (TCO) films on a glass substrate, a wide band gap semiconductor (most usually TiO_2 and ZnO nanocrytallintes), a ruthenium based dye, a redox electrolyte solution and a platinum (Pt) coated counter electrode. Efficient functioning of such devices is based on the ultrafast electron injection from the photo-excited state of the dye molecule into the conduction band of the TiO_2, followed by rapid regeneration of the dye with suitable redox couple in the electrolyte. The counter electrode (CE) of DSCs, enabling the transfer of electrons from the external circuit back to the electrolyte redox couple and catalyze the triiodide reduction at the counter electrode/electrolyte interface, usually utilizes a thin Pt film on a conducting glass substrate.[5,6] Although many other materials such as carbon,[7,8] conductive polymer,[9,10] and some inorganic compounds[11,12] have been introduced as inexpensive alternatives, Pt is still the cornerstone material because of its highly catalytic activity and superior chemical and electrochemical stabilities.

Recently, to improve the mechanical rigidity and stability of the electrocatalyst, bilayer films such as Pt/Ti,[13] Pt/NiO,[14] Pt/TiO_2,[15] and Pt/NiP[16] have been prepared through vacuum sputtering or thermal decomposition methods and applied as the CE of DSCs. However, these methods normally require complex facilities and operation procedures and thus are not suitable for large-scale production. More lately, mesoporous Nb-doped TiO_2 film was prepared by supramolecular templating with amphiphilic triblock copolymers on a transparent conducting FTO glass and served as the supporting substrate for conventional thermal decomposed Pt nanoparticles.[17] Interesting, it was observed that the charge transfer resistance was greatly reduced and the exchange current density was increased as the

Received: June 21, 2011
Accepted: September 2, 2011
Published: September 02, 2011

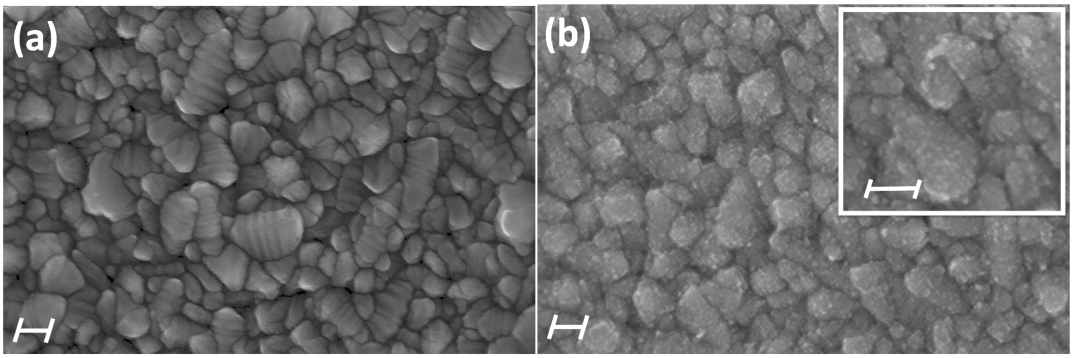

Figure 1. FESEM images of the surface morphologies of (a) Pt A and (b) Pt B (inset shows a magnified view) counter electrode with scale bar of 100 nm.

result of a larger active surface area of Pt in the mesoporous Nb-doped TiO_2. Therefore, developing a facile method to fabricate such bilayer-structure CEs with high electrocatalytic activity is of fundamental interest and imperative for the development of commercial large-scale DSC devices.

On the other hand, titanium tetrachloride treatment on the TiO_2 electrodes of DSCs is a widely-used post-treatment technique that greatly improves the photovoltaic performance,[18,19] which usually results in an improvement in photocurrent density, normally between 10% and 30%. Recently, this procedure has also been successfully applied into the TiO_2 mesosponge[20] and the mesoporous TiO_2 beads based photoanode.[21] However, to the best knowledge of the authors, this facile technique has never been exploited to prepare the CE of DSCs up to date.

It is well-known that the available catalytic surface in the electrode plays a crucial role in determining the overall catalytic property. Herein, we report the utilization of $TiCl_4$ treatment on the fluorine-doped tin oxide (FTO) coated glass substrates by a facile chemical bath method, serving as the scaffolding underlayer for the platinized CE of DSC for the first time, and aiming to assure a higher number density of catalytic sites. The surface structure, the catalytic activity toward triiodide reduction, as well as the photovoltaic responses of device incorporated with this novel bilayer CE were investigated. Meanwhile, conventional sputtered Pt electrode was also fabricated for comparison. Interestingly, as the result of a larger active surface area of Pt supported in the bilayer structure, the Pt/TiO_2 bilayer CE exhibited superior electrocatalytic activity toward triiodide reduction compared with that of the conventional sputtered Pt electrode. Consequently, device with this novel bilayer CE conferred notably improved fill factor and energy conversion efficiency under standard illumination.

2. MATERIALS AND METHODS

All chemicals and solvents used were of analytical grade. *N*-Methylbenzimidazole (NMBI) and guanidinium thiocyanate (GNCS) (Aldrich, USA), 1-propyl-3-methylimidazolium iodide (Merck AG, Germany), N719 dye ($[(C_4H_9)_4N]_2[Ru(II)L_2(NCS)_2]$, where L=2,2′-bipyridyl-4,4′-dicarboxylic acid, ruthenium TBA535, Solaronix, Switzerland) were used without further purification. Conducting glass plates (FTO glass, sheet resistance: 12 Ω/□, Nippon Sheet Glass Co., Japan) were used as the electrode substrates.

Conventional sputtered Pt CE (denoted as Pt A) was prepared by an ion sputtering coater (SBC-12, KYKY Technology Development Ltd., China) with duration of 20 sec for comparison. The thickness of the obtained Pt film was approximately 50 nm, as determined by the cross-section field emission scanning electron microscopy (FESEM) observation. Alternatively, to prepare the bilayer CEs (denoted as Pt B), cleaned FTO glasses (Nippon Sheet Glass Co., Japan) were first treated with 40 mM $TiCl_4$ aqueous solution at 70°C for 30 min. The resultant substrate was rinsed with water and ethanol subsequently and sintered at 500°C for 30 min. Afterwards, the $TiCl_4$ treated FTO glass was sputtered by Pt with the same thickness aforementioned. Sealed DSC devices were fabricated according to our previous reports, except that TiO_2 paste made from the commercial P25 nanoparticles was employed in current work.[22,23] Briefly, commercial P25 nanoparticles were mixed with terpineol and a viscous solution of ethyl cellulose in ethanol. After removing ethanol with a rotary-evaporator, TiO_2 paste consisting of 18% TiO_2 nanoparticles and 9% ethyl cellulose in terpineol was prepared. The thickness of the TiO_2 film and active area of all devices were 12 μm and 0.16 cm^2, respectively. The electrolyte was 1.0 M 1-propyl-3-methylimidazolium iodide, 0.03 M I_2, 0.5 M *N*-Methylbenzimidazole and 0.1 M guanidinium thiocyanate in acetonitrile.

The morphologies of the obtained CEs were characterized by field emission scanning electron microscopy (FE-SEM, LEO-1530, Germany) and atomic force microscopy (AFM, SEIKO SPA400, Japan). Pt loading of the CE was quantified by the X-ray fluorescence spectrometer (XRF-1800, Shimadzu, Japan). Sheet resistances of the CEs were tested by four-point probe measurement (SX1934, Baishen Technology, China). To assess the corresponding catalytic performance of different CEs, we carried out cyclic voltammetry (CV) measurements in a three-electrode cell on a CHI 650C potentiostat-galvanostat (CH Instruments Inc., USA) at a scanning rate of 50 mV s^{-1}. The prepared CEs, a Pt foil electrode and a saturated calomel electrode (SCE) were used as the working electrode, the counter electrode and the reference electrode, respectively. The electrolyte was acetonitrile containing 0.1 M $LiClO_4$ as the supporting electrolyte, 10 mM LiI and 1 mM I_2 as the redox couple. Specifically, the electrochemical active surface area of the as-prepared CEs was verified by measuring CV with the same configuration aforementioned between 1.4 and −0.24 V (vs. SCE)in an aqueous solution of 0.5 M H_2SO_4. Before scanning, it was deaerated by continuous bubbling of argon gas for 30 min. Furthermore, the charge-transfer resistance (R_{ct}) across the counter electrode/electrolyte interface was investigated by means of electrochemical impedance spectroscopy (EIS) with the symmetrical thin-layer cells method.[22,23] The photocurrent-photovoltage (*J*-*V*) characteristics of DSCs were measured with a digital source meter (2400, Keithley Instruments, USA) under AM 1.5 illumination (100 mW cm^{-2}), which was realized by a solar simulator (91192, Oriel, USA, calibrated with a standard crystalline silicon solar cell).

3. RESULTS AND DISCUSSIONS

Apparently, a large active surface area and excellent conductivity of the catalyst are highly desirable for an efficient catalytic electrode.

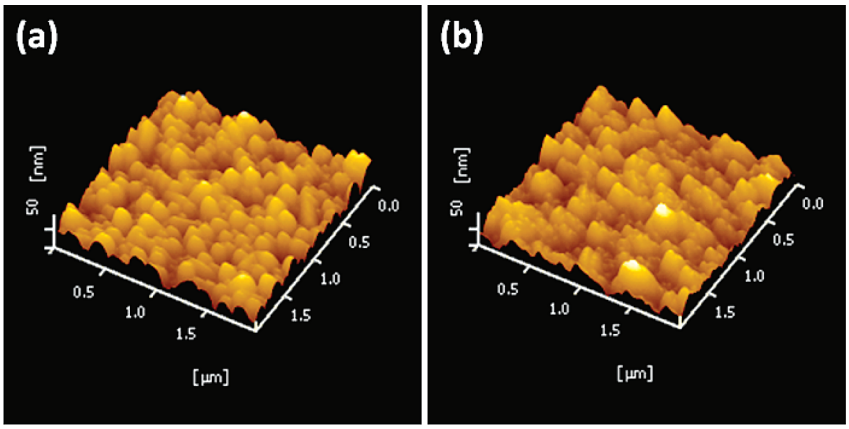

Figure 2. Three-dimensional AFM images of (a) Pt A and (b) Pt B counter electrodes with an area of 2 × 2 μm^2.

To this end, researchers have introduced various nanostructured materials as the catalyst supports in fuel cells, such as carbon nanotubes (CNTs),[24] ordered mesoporous carbon (OMC),[25] and most recently, graphene nanosheets,[26] giving rise to significantly enhanced electrocatalytic activity when compared with planar catalyst. However, little attention have been paid to the structure-engineered counter electrode in DSCs. Herein, $TiCl_4$ treatment has been employed to construct a rough scaffolding underlayer for the platinized counter electrode of DSCs for the first time.

The surface morphologies and roughness factors of the obtained composite CE as well as conventional sputtered Pt CE were observed by means of FESEM and AFM. Figure 1 shows the typically FESEM surface morphologies of Pt A (conventional sputtered Pt) and Pt B ($TiCl_4$ treated bilayer-structure) counter electrode. It is apparent from the FESEM images that hundreds of nanoparticles with a diameter up to a hundred nanometers were arranged compactly on the FTO conductive glass surface in Pt A CE (Figure 1a). Interestingly, when the FTO glass was first treated with the $TiCl_4$ solution, numerous Pt nanoparticles with sizes of ca. 10 nm are homogeneously distributed on the surface, indicating the existence of the rough scaffolding underlayer resulted from the $TiCl_4$ treatment process (Figure 1b). As depicted in the inset of Figure 1b, a magnified view of such Pt nanoparticles clearly demonstrated the nanosize diameter and aggregate-network form, thus affording a high number density of catalytic sites. As determined by the cross-section FESEM observation, the average thickness of the TiO_2 underlayer was approximately 80 nm. Furthermore, the surface roughness factor of the obtained bilayer Pt film, as verified by AFM observation (Figure 2b), was considerably enhanced in comparison with that of Pt A CE (Figure 2a). The root mean square surface roughness factor (R_{rms}) of Pt A CE was determined to be 13.13 nm and that of Pt B CE was increased to 14.63 nm after the introduction of the scaffolding underlayer. Recently, similar enhancement of the surface roughness factor has also been revealed in nanoparticular Pt CE prepared by a bottom-up wet chemical synthetic approach when compared with the conventional Pt CE prepared by sputtering deposition and thermal decomposition methods.[27] Therefore, it can be inferred from the surface morphologies that the bilayer film is expected to increase the effective electrochemical surface area of the deposited Pt films, which is crucial for high electrocatalytic activity of the CEs.

The electrochemical active surface area (EAS) of the Pt CE is one key parameter to determine the catalytic activity,[28] which has been evaluated by the CV measurement in H_2SO_4 solution in the present study. As shown in Figure 3, Q_1 and Q_2 represent the amount of charge exchanged during the electro-adsorption and desorption of H_2 on Pt sites and the intermediate fill area indicates the contribution of the double layer charge.[29] EAS of the obtained CEs was calculated by equation[28,29]

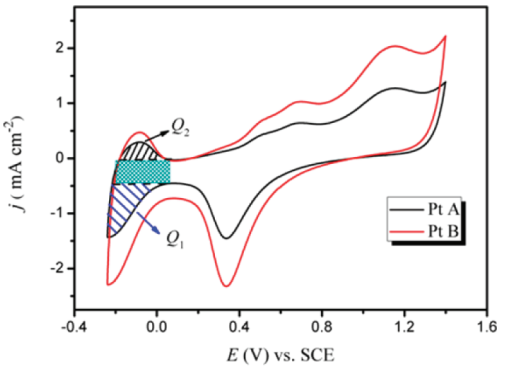

Figure 3. Cyclic voltammograms of different counter electrodes inaqueous solution of 0.5 M H_2SO_4, Q_1, and Q_2 represent the amount of charge exchanged during the electro-adsorption and -desorption of H_2 on Pt sites and the intermediate fill area is the contribution of double layer charge.

$$EAS = \frac{Q_H}{[Pt]0.21} = \frac{Q_1 + Q_2}{2[Pt]0.21} \quad (1)$$

where [Pt] is the Pt loading (mg cm^{-2}) of the electrode, Q_H is the Coulombic charge for hydrogen desorption (which is the mean value of Q_1 and Q_2 in this case) and 0.21 is the charge required to oxidize a monolayer of H_2 on bright Pt (mC cm^{-2}).[29,30] As tabulated in Table 1, the Pt loading of the CE was quantified by the XRF analyses, which was 5.69 and 5.94 μg cm^{-2} for Pt A CE and bilayer Pt B CE, respectively. Notably, the derived EAS of the bilayer Pt/TiO_2 CE was increased from 51.95 m^2 g^{-1} (Pt A CE) to 62.14 m^2 g^{-1}, which coincided well with the higher surface roughness of the bilayer CE as observed by FESEM and AFM.

In addition, the catalytic performance of CEs was analyzed by CV measurements in acetonitrile containing $LiClO_4$ as the supporting electrolyte and LiI+I_2 as the redox couple. Obviously, two well-defined reduction peaks and the corresponding oxidation peaks were visible when both of the CEs were

Table 1. Properties of Different Counter Electrodes and Detailed Photovoltaic Performance of Corresponding Devices Measured under AM 1.5 Illuminations (100 mW cm^{-2})[a]

CE	Pt loading (ug cm^{-2})	EAS (m^2 g^{-1})	R_{sq} (Ω/□)	R_s (Ω cm^2)	R_{ct} (Ω cm^2)	W_s (Ω cm^2)	V_{oc} (mV)	J_{sc} (mA cm^{-2})	*FF*	η (%)
A	5.69	51.95	12.7	2.64	2.46	1.02	756	13.97	0.60	6.37
B	5.94	62.14	12.9	2.53	0.62	0.98	754	14.03	0.67	7.09

[a] EAS, electrochemical active surface area; R_{sq}, sheet resistances measured from the four-point probe tests; R_s, R_{ct}, and W_s, the series resistance, charge transfer resistance, and Warburg diffusion resistance in the electrolyte fitted from the EIS measurements, respectively; V_{oc}, open-circuit voltage; J_{sc}, short-circuit photocurrent density; *FF*, fill factor; η, overall conversion efficiency.

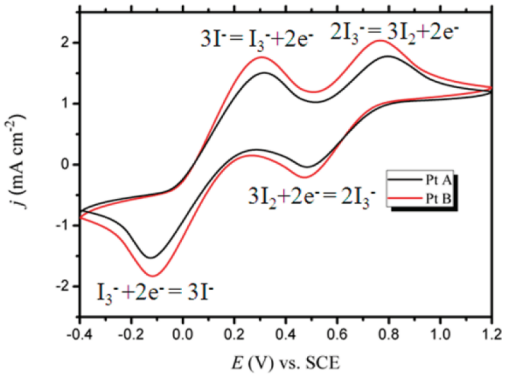

Figure 4. Cyclic voltammograms of different counter electrodes in acetonitrile solution containing 0.1 M $LiClO_4$, 10 mM LiI, and 1 mM I_2.

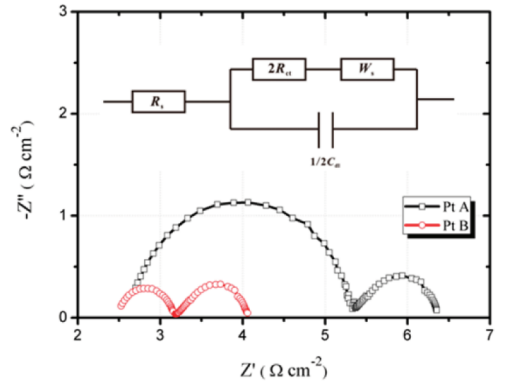

Figure 5. Nyquist plots of symmetrical cells with different counter electrodes. The Randles circuit is shown in the inset, including a component R_s = series resistance, R_{ct} = charge-transfer resistance, C_{dl} = double layer capacitance, and W_s = Warburg diffusion impedance. The cells were measured without applied voltage (0 V) in the dark.

used as the working electrodes. As indicated in Figure 4, in an anodic sweep direction, iodide is oxidized to triiodide (anodic peak 1) and then to iodine (anodic peak 2). Conversely, iodine is first reduced to triiodide (cathodic peak 1) and then to iodide (cathodic peak 2) when the potential scanning direction is reversed. The oxidation and reduction profiles of I^-/I_3^- for the two different CEs were quite similar while almost 20% larger current density was observed when bilayer Pt B CE was used, indicating the superior electrocatalytic activity of Pt/TiO_2 bilayer electrode, which was directly attributed to the formation of nanosized Pt crystalline on the rough scaffolding underlayer and significantly enhanced EAS (19.6%) of the CE.

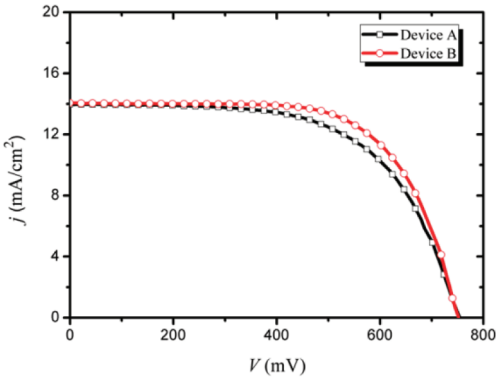

Figure 6. *J*−*V* characteristics of devices measured under AM 1.5 illumination (100 mW cm^{-2}).

Apart from the electrochemical active surface area (EAS) aforementioned, an excellent electrical conductivity is also indispensable to an efficient CE. In the present study, sheet resistances (R_{sq}) of the CEs were firstly tested by four-point probe measurement to check the impact of the introduction of a TiO_2 rough scaffolding underlayer on the electrical property. As depicted in Table 1, the R_{sq} of the Pt A and composite Pt B electrode was almost unchanged, which was 12.7 and 12.9 Ω/□, respectively. Such a behavior suggested that the sheet resistance of a CE is directly dominated by the conducting substrate, for instance, FTO in this study, which was also indicative of the ultrathin thickness of the intermediate scaffolding underlayer.

Electrochemical impedance spectroscopy (EIS) is extensively employed to investigate the electronic kinetic performance of the electrodes in DSCs.[31,32] Figure 5 presents the corresponding Nyquist spectra of symmetrical cells with different CEs. It is generally concluded that in the order of increasing frequency, the response can be attributed to the Warburg diffusion processes in the electrolyte and charge transfer at the CE/electrolyte interface. Fitted with the Randles equivalent circuit shown in the inset, the charge transfer resistance (R_{ct}) of the bilayer Pt B CE as shown in Table 1 was 0.62 Ω cm^2, a value only one forth of that for the pure Pt CE (2.46 Ω cm^2), further highlighting the superior electrocatalytic activity of the bilayer electrodes for the reduction of triiodide ions. Nevertheless, the variation in series resistance (R_s) and the Warburg diffusion resistance in the electrolyte (W_s) was trivial. It is worthy to address that the R_{ct} of the presented bilayer Pt/TiO_2 CE was considerably smaller than that of the recently reported carbon[7] and inorganic compounds analogues.[11,12]

To assess the potential application of the facilely prepared bilayer CEs, devices were assembled with the same N719 sensitized TiO_2 electrodes. Figure 6 demonstrates the characteristic *J*−*V* curves for devices with Pt A and B CE measured under

AM 1.5 illumination and the detailed photovoltaic parameters were tabulated in Table 1. The photovoltaic charcteristics of device A with Pt A CE were open-circuit voltage (V_{oc}), 756 mV; short-circuit photocurrent density (J_{sc}), 13.97 mA cm^{-2}; fill factor (*FF*), 0.60; and overall conversion efficiency (η), 6.37%, whereas those of device B with bilayer CE were V_{oc}, 754 mV; J_{sc}, 14.03 mA cm^{-2}; *FF*, 0.67; and η, 7.09%. It was apparent that the enhancement of the η was directly originated from the *FF* increase. It is important to note that the *FF* is attenuated by the total series resistance of the cell, which includes the sheet resistances of the substrate and counter electrode, electron transport resistance through the photoanode, ion transport resistance, and the charge-transfer resistance at the counter electrode.[33] Therefore, the *FF* enrichment in the current work can be mainly profited from the superior electrocataltic activity of the bilayer CE and consequent significantly reduced charge-transfer resistance across the CE/electrolyte interface. The obtained conversion efficiency is of great advantage when compared to that of other bilayer CE based devices, such as Pt/NiO,[13] Pt/Ti,[14] and Pt/TiO_2,[15] especially taking the facile fabrication process into consideration.

4. CONCLUSIONS

In summary, titanium tetrachloride treatment has been successfully exploited to form highly electrocatalytic bilayer-structure counter electrode in DSCs for the first time, through forming a rough scaffolding underlayer resulted from the controlled hydrolysis of $TiCl_4$ solution. The surface structure and electrocatalytic property of the obtained composite CE was investigated by FESEM, AFM, CV as well as EIS techniques. Promisingly, the Pt/TiO_2 bilayer CE exhibited higher surface roughness factor, larger electrochemical surface area as well as superior electrocatalytic activity toward triiodide reduction compared with that of the conventional pure sputtered Pt electrode. Device with this novel bilayer CE evoked considerably improved fill factor and energy conversion efficiency under standard illumination. Therefore, the interfacial roughness engineering is a powerful means to enhance the electrocatalytic activity of counter electrode, and the current study indicates that commonly-applied $TiCl_4$ treatment paves a novel and facile way to prepare high-electrocatalytic bilayer CE in DSCs.

AUTHOR INFORMATION

Corresponding Author

*E-mail: Hong-lin@tsinghua.edu.cn. Fax/Tel: +86 10-62772672.

ACKNOWLEDGMENT

The International Cooperation MOST-JST Program Fund (2010DFA61410), the MOST International S&T Cooperation Program of China (2010DFB23160) and the Sanjiangyuan Scientific Program of Qinghai Science & Technology Department (2010−N-S03) are acknowledged for financial support.

REFERENCES

(1) O'Regan, B.; Grätzel, M. *Nature* **1991**, *353*, 737–740.
(2) Grätzel, M. *Acc. Chem. Res.* **2009**, *42*, 1788–1798.
(3) Hagfeldt, A.; Boschloo, G.; Sun, L. C.; Kloo, L.; Pettersson, H. *Chem. Rev.* **2010**, *110*, 6595–6663.
(4) Chiba, Y.; Islam, A.; Watanabe, Y.; Komiya, R.; Koide, N.; Han, L. *Jpn. J. Appl. Phys.* **2006**, *45*, L638–L640.
(5) Papageorgiou, N. *Coord. Chem. Rev.* **2004**, *248*, 1421–1446.
(6) Grätzel, M. *Prog. Photovolt. Res. Appl.* **2006**, *14*, 429–442.
(7) Ramasamy, E.; Lee, J. *Carbon* **2010**, *48*, 3715–3720.
(8) Ghamouss, F.; Pitson, R.; Odobel, F.; Boujtita, M.; Caramori, S.; Bignozzi, C. A. *Electrochim. Acta* **2010**, *55*, 6517–6522.
(9) Hong, W.; Xu, Y.; Lu, G.; Li, C.; Shi, G. *Electrochem. Commun.* **2008**, *10*, 1555–1558.
(10) Li, Q.; Wu, J.; Tang, Q.; Lan, Z.; Li, P.; Lin, J.; Fan, L. *Electrochem. Commun.* **2008**, *10*, 1299–1302.
(11) Wang, M. K.; Anghel, A. M.; Marsan, B.; La, N-L. C.; Pootrakulchote, N.; Zakeeruddin, S. M.; Grätzel, M. *J. Am. Chem. Soc.* **2009**, *131*, 15976–15977.
(12) Li, G. R.; Wang, F.; Jiang, Q. W.; Gao, X. P.; Shen, P. W. *Angew. Chem., Int. Ed.* **2010**, *49*, 3653–3656.
(13) Ikegami, M.; Miyoshi, K.; Miyasaka, T.; Teshima, K.; Wei, T. C.; Wan, C. C.; Wang, Y. Y. *Appl. Phys. Lett.* **2007**, *90*, 153122–153124.
(14) Kim, S.-S.; Park, K.-W.; Yum, J.-H.; Sung, Y.-E. *Sol. Energy Mater. Sol. Cells* **2006**, *90*, 283–290.
(15) Kim, S.-S.; Park, K.-W.; Yum, J.-H.; Sung, Y.-E. *J. Photochem. Photobiol. A: Chem.* **2007**, *189*, 301–306.
(16) Wang, G.; Lin, R.; Lin, Y.; Li, X.; Zhou, X.; Xiao, X. *Electrochim. Acta* **2005**, *50*, 5546–5552.
(17) Hasin, P.; Alpuche-Aviles, M. A.; Li, Y.; Wu, Y. *J. Phys. Chem. C* **2009**, *113*, 7456–7460.
(18) Barbe, C. J.; Arendse, F.; Comte, P.; Jirousek, M.; Lenzmann, F.; Shklover, V.; Gratzel, M. *J. Am. Ceram. Soc.* **1997**, *80*, 3157–3171.
(19) Park, N. G.; Schlichthörl, G.; van de Lagemaat, J.; Cheong, H. M.; Mascarenhas, A.; Frank, A. J. *J. Phys. Chem. B* **1999**, *103*, 3308–3314.
(20) Kim, D.; Roy, P.; Lee, K.; Schmuki, P. *Electrochem. Commun.* **2010**, *12*, 574–578.
(21) Sauvage, F.; Chen, D.; Comte, P.; Huang, F.; Heiniger, L.-P.; Cheng, Y.-B.; Caruso, R. A.; Grätzel, M. *ACS Nano* **2010**, *4*, 4420–4425.
(22) Hao, F.; Lin, H.; Zhang, J.; Li, J. *J. Power Sources* **2011**, *196*, 1645–1650.
(23) Hao, F.; Lin, H.; Zhang, J.; Zhuang, D.; Liu, Y.; Li, J. *Electrochim. Acta* **2010**, *55*, 7225–7229.
(24) Antolini, E. *Appl. Catal. B* **2009**, *88*, 1–24.
(25) Chang, H.; Joo, S. H.; Pak, C. *J. Mater. Chem.* **2007**, *17*, 3078–3088.
(26) Li, Y.; Tang, L.; Li, J. *Electrochem. Commun.* **2009**, *11*, 846–849.
(27) Calogero, G.; Calandra, P.; Irrera, A.; Sinopoli, A.; Citro, I.; Marco, G. D. *Energy Environ. Sci.* **2011**, *4*, 1838–1844.
(28) Zhang, F.; Ceder, M.; Inganas, O. *Adv. Mater.* **2007**, *19*, 1835–1838.
(29) Pozio, A.; Francesco, M. D.; Cemmi, A.; Cardellini, F.; Giorgi, L. *J. Power Sources* **2002**, *105*, 13–19.
(30) Lee, S. J.; Mukerjee, S.; McBreen, J.; Rho, Y. W.; Kho, Y. T.; Lee, T. H. *Electrochim. Acta.* **1998**, *43*, 3693–3701.
(31) Fabregat-Santiago, F.; Bisquert, J.; Palomares, E.; Otero, L.; Kuang, D.; Zakeeruddin, S. M.; Grätzel, M. *J. Phys. Chem. C* **2007**, *111*, 6550–6560.
(32) Wang, Q.; Ito, S.; Grätzel, M.; Fabregat-Santiago, F.; Mora-Sero, I.; Bisquert, J.; Bessho, T.; Imai, H. *J. Phys. Chem. B* **2006**, *110*, 25210–25221.
(33) Hamann, T. W.; Jensen, R. A.; Martinson, A. B. F.; Ryswykac, H. V.; Hupp, J. T. *Energy Environ. Sci.* **2008**, *1*, 66–78.